JGR Space Physics

RESEARCH ARTICLE
10.1029/2020JA028929

Special Section:
Geospace multi-point observations in Van Allen Probes and Arase era

Preliminary Statistical Comparisons of Spin-Averaged Electron Data From Arase and Van Allen Probes Instruments

Mátyás Szabó-Roberts[1,2], Yuri Y. Shprits[1,2,3], Hayley J. Allison[1], Ruggero Vasile[1], Artem G. Smirnov[1,2], Nikita A. Aseev[1,2], Alexander Y. Drozdov[2], Yoshizumi Miyoshi[4], Seth G. Claudepierre[3,5], Satoshi Kasahara[6], Shoichiro Yokota[7], Takefumi Mitani[8], Takeshi Takashima[8], Nana Higashio[8], Tomo Hori[4], Kunihiro Keika[6], Shun Imajo[4], and Iku Shinohara[8]

[1]GFZ German Research Centre for Geosciences, Helmholtz Centre Potsdam, Potsdam, Germany, [2]Institute of Physics and Astronomy, University of Potsdam, Potsdam, Germany, [3]Department of the Earth, Planetary and Space Sciences, University of California, Los Angeles, CA, USA, [4]ISEE, Nagoya University, Nagoya, Japan, [5]Space Sciences Department, The Aerospace Corporation, El Segundo, CA, USA, [6]School of Science, University of Tokyo, Tokyo, Japan, [7]Osaka University, Toyonaka, Japan, [8]Japanese Aerospace Exploration Agency, Tokyo, Japan

Abstract Following the end of the Van Allen Probes mission, the Arase satellite offers a unique opportunity to continue in-situ radiation belt and ring current particle measurements into the next solar cycle. In this study we compare spin-averaged flux measurements from the MEPe, HEP-L, HEP-H, and XEP-SSD instruments on Arase with those from the MagEIS and REPT instruments on the Van Allen Probes, calculating Pearson correlation coefficient and the mean ratio of fluxes at L* conjunctions between the spacecraft. Arase and Van Allen Probes measurements show a close agreement over a wide range of energies, observing a similar general evolution of electron flux, as well as average, peak, and minimum values. Measurements from the two missions agree especially well in the $3.6 = L^* \leq 4.4$ range where Arase samples similar magnetic latitudes to Van Allen Probes. Arase tends to record higher flux for energies <670 keV with longer decay times after flux enhancements, particularly for $L^* < 3.6$. Conversely, for energies >1.4 MeV, Arase flux measurements are generally lower than those of Van Allen Probes, especially for $L^* > 4.4$. The correlation coefficient values show that the >1.4 MeV flux from both missions are well correlated, indicating a similar general evolution, although flux magnitudes differ. We perform a preliminary intercalibration between the two missions using the mean ratio of the fluxes as an energy- and L*- dependent intercalibration factor. The intercalibration factor improves agreement between the fluxes in the 0.58–1 MeV range.

Key Points:

- MEPe, HEPH, HEPL, XEPSSD, and MAGEIS/REPT show a good correlation at energies above 300 keV and $3 < L^* < 4.6$
- Flux measurements at the same energy from the two missions are highly comparable in magnitude
- Intercalibration via energy- and L*-dependent factors improves the agreement between Arase and RBSP

Supporting Information:

Supporting Information may be found in the online version of this article.

Correspondence to:

M. Szabó-Roberts,
matszabo@gfz-potsdam.de

Citation:

Szabó-Roberts, M., Shprits, Y. Y., Allison, H. J., Vasile, R., Smirnov, A. G., Aseev, N. A., et al. (2021). Preliminary statistical comparisons of spin-averaged electron data from Arase and Van Allen Probes instruments. *Journal of Geophysical Research: Space Physics*, *126*, e2020JA028929. https://doi.org/10.1029/2020JA028929

Received 13 NOV 2020
Accepted 15 JUN 2021

1. Introduction

Following the discovery of Earth's Van Allen belts, numerous spacecraft have been launched to supply ongoing scientific investigation of the radiation belts with appropriate data (Li & Hudson, 2019). From 2012–2019, the Van Allen Probes mission (also known as Radiation Belt Storm Probes, RBSP) provided a plethora of data, aiming to answer some of the most persistent questions in the field, and resulted in several key discoveries over the lifetime of the project. Examples include the discovery of a temporary three-belt structure (Baker et al., 2013), showing that the inner Van Allen belt does not contain electrons with energy >1 MeV (Fennell et al., 2015), and providing insight into various wave-particle interactions and dynamics (e.g., Agapitov et al., 2016; Breneman et al., (2015); Foster et al., 2017; Xiao et al., 2014, 2015; Yuan & Zong, 2019).

A currently active mission is the Exploration of Energization and Radiation in Geospace (ERG/Arase) project, launched in 2016 (Miyoshi, Shinohara, et al., 2018), which provides comparable instrumentation to RBSP and slightly extended sampling in L (discussed in Section 2). This opens up the possibility of direct comparisons between Arase and other long-term missions in Earth's radiation belts and ring current at higher L, such as the Geostationary Operational Environmental Satellites (GOES: Davis, 2007), the Los Alamos National Laboratory geostationary satellites (LANL-GEO/GEO: Reeves et al., 1997), and the recently

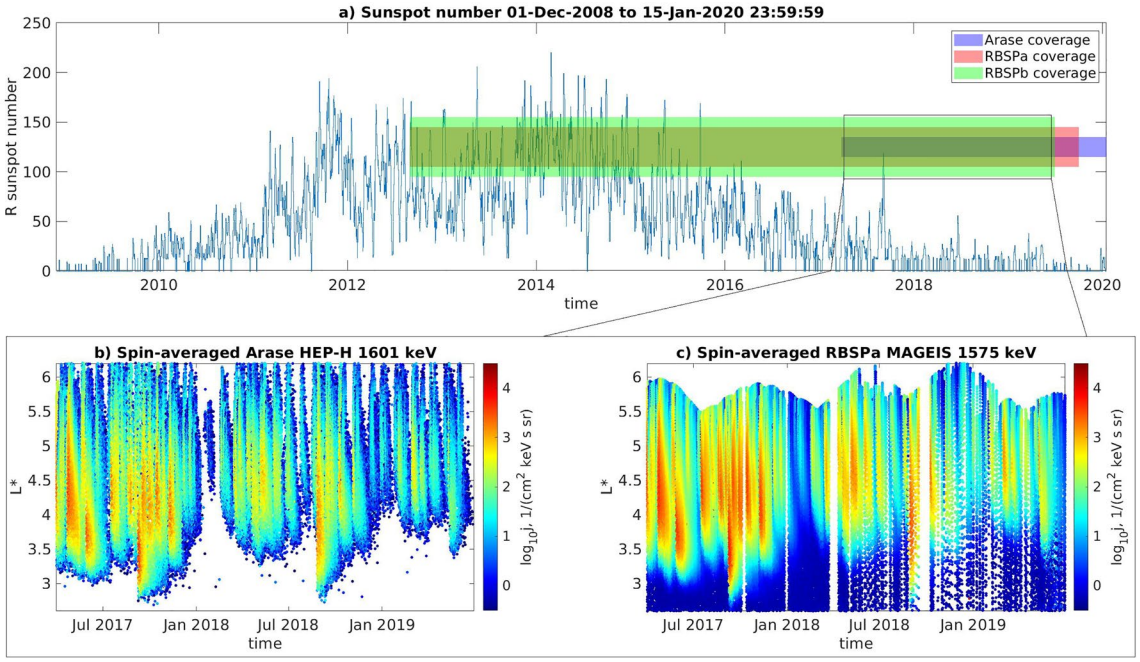

Figure 1. (a) Daily averaged sunspot number as a function of time for solar cycles 24–25. The red, green, and blue boxes denote the coverage of RBSPa, RBSPb, and Arase respectively. (b) Spin-averaged electron flux measured by Arase HEP-H for the 1.6 MeV channel. (c) Spin-averaged electron flux measured by RBSPa MagEIS for the 1.575 MeV channel. Observations on (b–c) are presented as a function of time and L* (for a local 90° pitch angle channel) computed using the T89 magnetic field model (Tsyganenko, 1989).

background-corrected Cluster electron measurements, already cross-calibrated with the RBSP (Smirnov et al., 2019, 2020).

As highlighted in Friedel et al. (2005), using the Combined Release and Radiation Effects Satellite (CRRES: Vampola, 1992) to intercalibrate GEO and GPS data, spacecraft with large L coverage can act as a reference to establish an intercalibration even between missions that would not otherwise have a statistically significant amount of conjunctions in L. The L coverage of Arase enables the data set to be used in a similar manner, for example, between the RBSP and GOES missions that have very few L* conjunctions due to RBSP being generally near the equator in an orbit that has its apogee inside the geostationary orbit (Baker et al., 2019). This principle can also be extended to interplanetary missions on a heliospheric scale, as demonstrated in Roussos et al. (2020).

Recent data assimilation studies (Cervantes et al., 2020) and assimilative real-time radiation belt forecasting (Shprits & Michaelis, 2018) aim to use intercalibrated data sets from multiple sources. A widely used intercalibration method is matching phase space densities at phase space coordinate conjunctions (Chen, 2005). In order to establish the intercalibration, these studies are either limited to missions that provide pitch angle resolved data and phase space density products (Boyd et al., 2018), or rely on assumptions about the pitch angle distribution of electron flux to compute phase space densities (Kellerman et al., 2014; Ni et al., 2011). Spin-averaged comparisons can be performed even in cases where no pitch angle resolved data are available, and intercalibrations based on spin-averaged comparisons have been shown to be in good agreement with intercalibrations obtained by matching phase space densities at phase space coordinate conjunctions (Friedel et al., 2005). On-orbit statistical comparisons of spin-averaged data are therefore be used to intercalibrate Arase to a wide range of satellite missions, and are a suitable a topic for future studies.

2. Data Sources

In order to identify and understand potential differences between the Arase and RBSP data sets, we perform a set of detailed comparisons. As shown on Figure 1a, there is a 27 months overlap between Arase and RBSP, which allows us to perform direct comparisons between data from the spacecraft. RBSP sampled

most of solar cycle 24, and the overlap period with Arase is toward the solar minimum. As it stands, Arase is set to continue providing data throughout the next cycle. Figures 1b and 1c demonstrates that the Arase and RBSP spin-averaged fluxes are, in general, comparable for the energy shown, and observe flux enhancements across a similar L* range. There is no low value background on most of Figure 1b, since the time binned Arase HEP-H flux data often contains negative flux values in regions where the instrument is measuring close to background level. The negative values in the original files are obtained by applying the count spectrum deconvolution matrices to raw counts, and are kept for averaging (such as time binning) to improve statistics.

A notable feature of the RBSP data set is the impressive energy coverage: 1 eV to 20 MeV across the Helium, Oxygen, Proton, and Electron mass spectrometer (HOPE: Funsten et al., 2013), Magnetic Electron Ion Spectrometer (MagEIS: Blake et al., 2013), and Relativistic Electron-Proton Telescope (REPT: Baker et al., 2012) instruments. Recent work has aimed to create a combined product from these instruments across all 72 energy channels (Boyd et al., 2019), and there is ongoing effort to further improve intercalibration between the instruments.

Across four electron instruments, Arase provides comparable energy coverage to the RBSP mission with 8 s nominal time resolution. The lowest energy instrument is the Low Energy Particle Experiments—electron analyzer (LEPe: Kazama et al., 2017), which is an electrostatic analyzer operating in the 20 eV–20 keV energy range with 32 energy channels.

The Medium Energy Particle Experiment—electron analyzer (MEPe) is another electrostatic analyzer measuring electrons with energies 7–87 keV with a field of view of 360° (azimuth) 3.5° (elevation), taking data at each of the 32 spin phases of the spacecraft (Kasahara et al., 2018).

For higher energies, Arase includes the two-unit High Energy Particle Experiment (HEP), consisting of silicon solid-state detectors operating over energies of 70 keV–1 MeV in 16 channels (Low unit, HEP-L), and 0.7–2 MeV in 11 channels (High unit, HEP-H). Both HEP-L and HEP-H have a field of view of 180° in a plane that contains the axis of the spinning of the spacecraft (latitudinal), and 10° in the plane perpendicular to the axis (longitudinal). HEP resolves the satellite spin in 16 spin phases, and thus has a resolution of 22.5° in the longitudinal direction.

For measurements of the highest end of the electron energy spectrum, the mission utilizes the two-unit Extreme Energy Particle Experiment (XEP) with a field of view of 20° that takes data in 16 spin phases during each satellite spin, consisting of the silicon solid-state detector array XEP-SSD in the 0.4–3.15 MeV energy range and the XEP-GSO scintillator (uncalibrated at the time of writing) nominally operating in the 6–20 MeV energy range (Higashio et al., 2018).

For this preliminary study, we choose to focus on the medium-to high-energy instruments and are therefore omitting HOPE and LEPe from the analysis. The energy coverage from the MEPe, HEP, XEP, MagEIS, and REPT instruments is shown on Figures 2a and 2b using 1 month of data from both missions, binned to a 5 min time grid, where we used median flux from each bin. As is also observed in Figures 1b and 1c, Figure 2 indicates that the instruments show flux enhancements in the same energy ranges for both missions. Both Arase and RBSP operate with energy channel definitions that are nearly evenly spaced in logarithm of energy. Example energy spectra from the two missions are shown on Figures 2c and 2d. Despite using data from four separate instruments, the Arase spectra in general show good agreement between overlapping energy channels as of the latest data release (v3_01 for HEP and v01_02 for MEPe), and the agreement is expected to improve even further with future releases (Miyoshi, Hori, et al., 2018).

A key difference between the two missions is the satellite orbit. As seen from Figure 3, the Van Allen Probes operate in a geostationary transfer orbit with perigee 618 km, apogee 30,414 km, and period 537 min. On average, the probes are ∼10° from the magnetic equator (Stratton et al., 2013), which allows the Van Allen Probes to accurately sample particles at most equatorial pitch angles (see Figure 3d). The vast majority of the data measured correspond to $L^* < 7$ as computed using the T89 magnetic field model (Figure 3b). Arase is similarly in an elliptical geostationary transfer orbit with perigee 400 km, apogee 32,000 km, and a period of 570 min, but it is on average ∼20° inclined from the magnetic equator, as seen in Figure 3 (Miyoshi, Shinohara, et al., 2018). Consequently, Arase samples higher latitudes and L-shells than RBSP, up to $L^* = 9$.

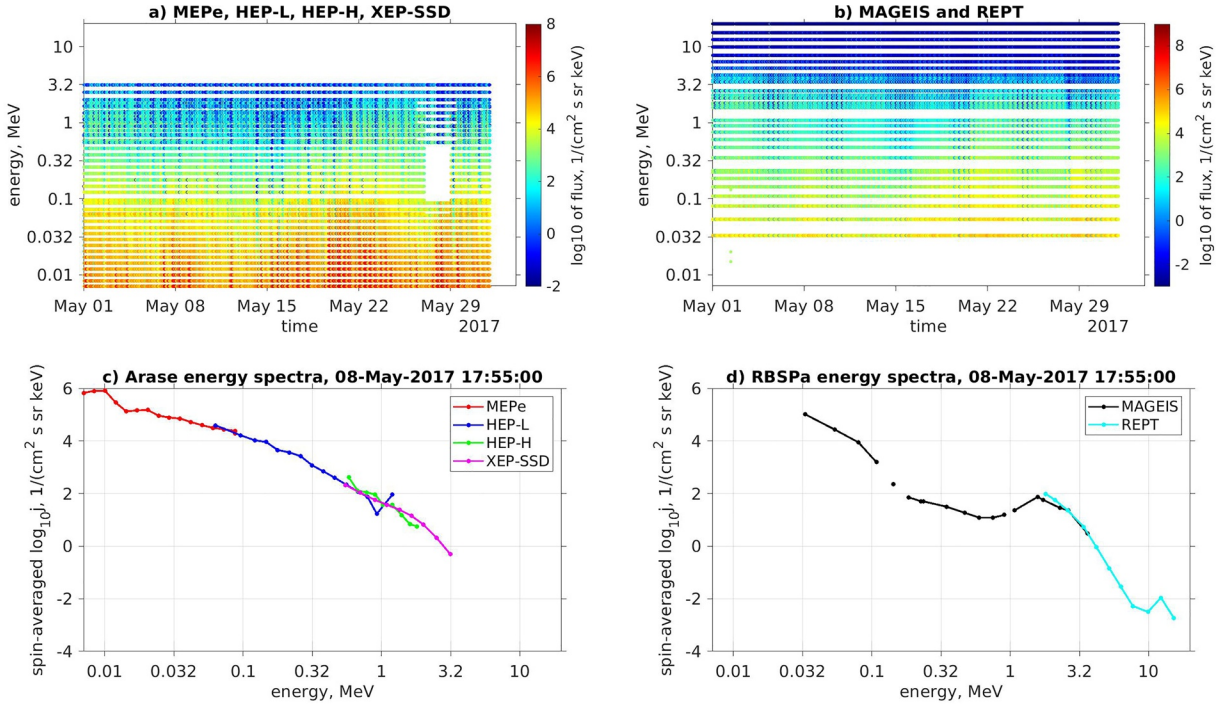

Figure 2. (a–b) Spin-averaged fluxes measured by the Arase MEPe, HEP, XEP-SSD and RBSPa MagEIS and REPT instruments in May 2017 for all energy channels as a function of time and base 10 logarithm of energy. (c–d) Combined energy spectrum from the electron instruments of Arase and RBSPa, respectively. The energy axes on all panels are plotted using a logarithmic scale.

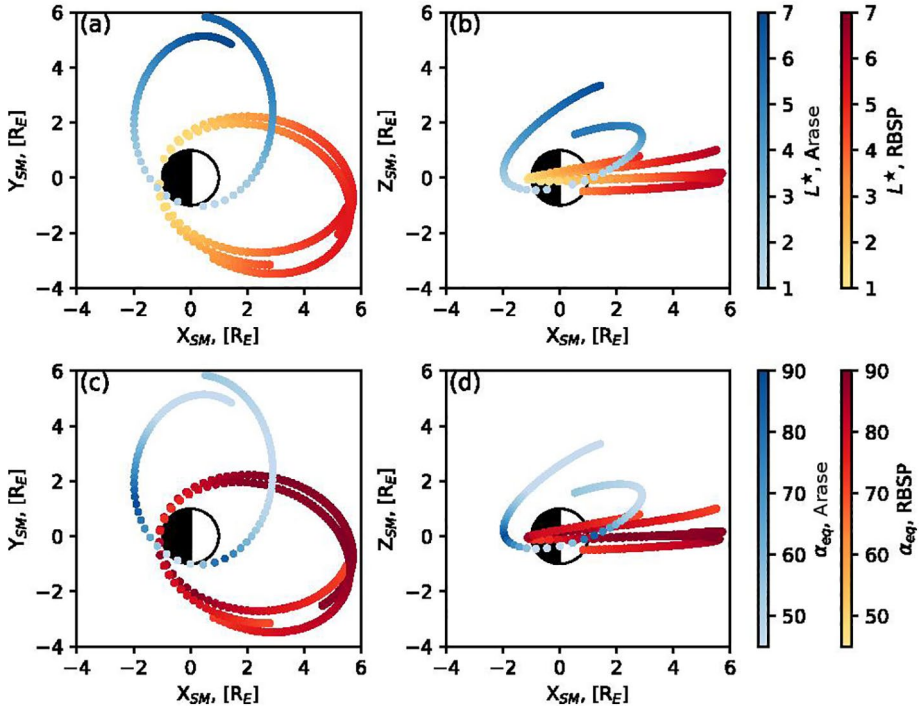

Figure 3. Example orbits of Arase and Radiation Belt Storm Probe (RBSP) for 2017/10/30 00:00 to 09:59. (a–b) 2D projections of satellite orbits colored by L* calculated for a local 90° pitch angle channel using the T89 magnetic field model. (c–d) 2D projections of satellite orbits colored by the maximum equatorial pitch angle the satellite can measure at each time.

At higher latitudes, the maximum equatorial pitch angle observed by Arase is much lower than 90° (Figure 3), and thus the instruments sample a smaller subset of the trapped electron population than a satellite positioned at the magnetic equator would. Since the RBSP orbits are less inclined, the satellites stay at lower latitudes and cover a broader range of equatorial pitch angles throughout their orbit. We would therefore expect the spin-averaged Arase product to be systematically lower than the spin-averaged RBSP flux for L* where Arase and RBSP sample different magnetic latitudes, and thus we impose an upper threshold of 10° on the difference in maximum equatorial pitch angle sampled by the spacecraft, as explained in Sections 2 and 4.

3. A Comparison of the Arase and RBSP Flux Data

In this study we compare Level 2 spin-averaged data from the Arase and RBSP missions. Since a background corrected data product is currently not available for the HEP and XEP measurements similar to that provided for MagEIS observations (Claudepierre et al., 2015), we use uncorrected MagEIS data for our comparisons. Our reasoning is discussed further in Section 5. We also provide our key figures reproduced with background corrected MagEIS data as supporting Figures S12–S15, which show no significant differences in the effectiveness of the intercalibration. We choose to interpolate RBSP measurements in energy to match the Arase energy channel definitions using linear interpolation in logarithm of energy. We restrict our comparisons to measurements where the maximum equatorial pitch angles observed by Arase and RBSP are within 10° of each other, in order to ensure that the satellite instruments sample a similar subset of the full angular distribution. The importance of this restriction is further discussed in Section 5, and Figures S10–S11 in the supporting information provide a demonstration of how this restriction on maximum equatorial pitch angle affects the magnetic latitudes we consider in our comparisons. We perform the same comparisons using data from both RBSPa and RBSPb, but since there is no significant difference between the results, we choose to only show results with RBSPa data in this paper. For the interested reader, we provide the equivalent of Figure 9 using RBSPb data as Figure S9 in the supporting information.

Figure 4 shows spin-averaged electron fluxes from the two missions binned in time to a 5 min grid with the median value calculated for each bin. We compare data at various energies at L* conjunctions, defined as the two satellites being within L* ± 0.1 of each other in a given 5 min time interval. The L* parameter is calculated for a local 90° pitch angle channel for both Arase and RBSP at each time interval with the T89 magnetic field model (Tsyganenko, 1989). At energies where both MagEIS and REPT provide flux data (i.e., ≥1.8 MeV), we have chosen to use MagEIS measurements, since at the time of writing, the REPT team suggested not using the REPT data for quantitative studies until the next data release.

From comparing Arase and RBSP data at these L* conjunctions, it can be seen that the measurements of the instruments from the two satellites are generally in good agreement for $3.6 = L^* \leq 4.4$. At lower energies (60–670 keV) and $L^* < 4$, Arase fluxes are consistently higher than RBSP fluxes. For the HEP-L instrument, this is largely caused by HEP-L having a higher background threshold than MagEIS, and frequently hitting that background threshold for the $L^* < 4$ measurements (demonstrated in Figure S2 in the supporting information). Other possible causes of this systematic difference are explored further in Section 5. At higher energies (>1.4 MeV), RBSP fluxes are typically higher than Arase fluxes, especially for $L^* > 4.4$. This can be explained by the fact that due to the orbit characteristics described in Section 1, Arase is likely to be on higher magnetic latitudes than RBSP for $L^* > 4.4$, and therefore consistently sample particle distributions with a lower maximum equatorial pitch angle (with the difference not exceeding our imposed restriction of 10°), and consequently measure lower values of spin-averaged flux. Aside from the magnetic latitude variation, other factors, such as the instrument background thresholds, may also contribute to this difference.

To examine the time evolution of the flux measured by both RBSP and Arase, we compare the flux on L* slices. We continue to use flux data binned to a 5 min time grid for this comparison. An energy range of 35 keV–2.5 MeV is considered. We present the plots for HEP-H in Figure 5, and the other Arase electron instruments in Figures S1–S3 in the supporting information. For the interested reader, a comparison with REPT data interpolated to the 2.5 MeV XEP-SSD channel is also included in the supporting information as Figure S8.

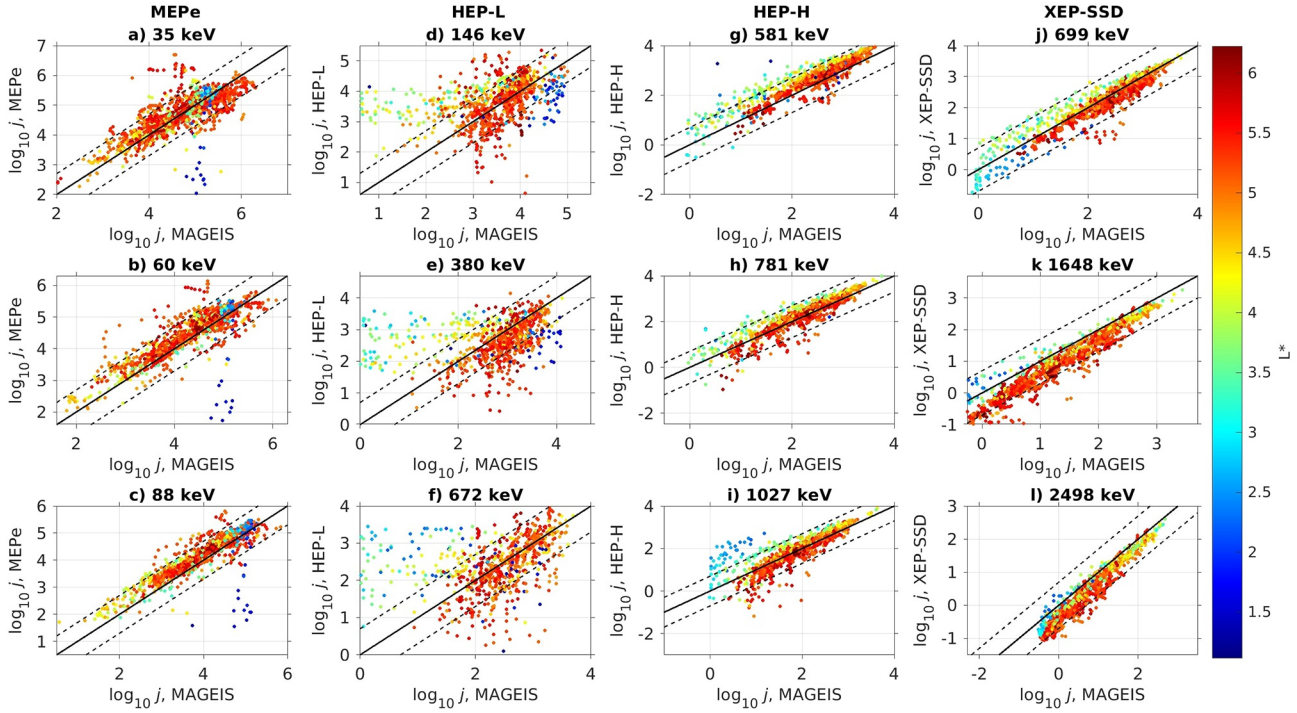

Figure 4. (a–l) Spin-averaged electron flux from Arase plotted against spin-averaged electron flux from RBSPa at L* conjunctions, in base 10 logarithm. L* conjunctions are defined as Arase and RBSPa being within L*±0.1 of each other in a given 5 min interval. RBSPa fluxes are interpolated to Arase energy channel definitions in energy. The color indicates L* computed for a local 90° pitch angle channel using the T89 magnetic field model for each measurement. For reference, the solid black line denotes one-to-one correspondence, and the black dashed lines denote agreement within a factor of 5.

Figure 5 shows that in general there is a good agreement between the measurements of the Arase and RBSP instruments. Although MagEIS has a lower noise floor than the Arase instruments at the same energies (demonstrated on Figures 5a, 5d and 5g where MagEIS clearly reads lower than Arase during quiet times), in general both missions record very similar enhancements during the time range studied. At L* = 3 (shown on Figures 5a, 5d and 5g), while RBSP and Arase instruments still record a similar flux level for the two notable enhancements, RBSP data shows a faster decay time after said enhancements in the 800–1400 keV energy range. This is discussed further in Section 5.

To obtain a more quantitative comparison, we calculate the Pearson correlation coefficients between Arase and RBSP fluxes at the same energy and L* (denoted as a and b in Equation 1, respectively).

$$\rho(a,b) = \frac{\sum_{i=1}^{n}(a_i - \overline{a})(b_i - \overline{b})}{\left(\sum_{i=1}^{n}(a_i - \overline{a})^2 \sum_{i=1}^{n}(b_i - \overline{b})^2\right)^{1/2}} \quad (1)$$

Equation 1: Pearson correlation coefficient $\rho(a, b)$ for 1D n-element data sets a and b, where $\overline{a}$ and $\overline{b}$ denote the mean of a and b, respectively.

To calculate correlation coefficients, we first binned the flux data for each energy channel into L* bins of width 0.2, then binned in time into 12 h intervals to create a time series of flux in each L* and energy bin. Increasing the time binning to 12 h intervals was necessary to ensure a sufficient number of intervals when both the Arase and RBSP data set has measurements in each L* and energy bin. We then calculated the Pearson correlation coefficient between Arase and RBSP measurements in the same L* and energy bin for both the flux values themselves and logarithm (base 10) of the flux values. We present the correlation coefficient for the logarithm of the flux measurements in Figure 6. Since the fluxes can range across five orders of magnitude for a given L* and energy channel, taking the logarithm reduces the influence of extreme values such as the background level, and the correlation is in general higher and more consistent across neighboring

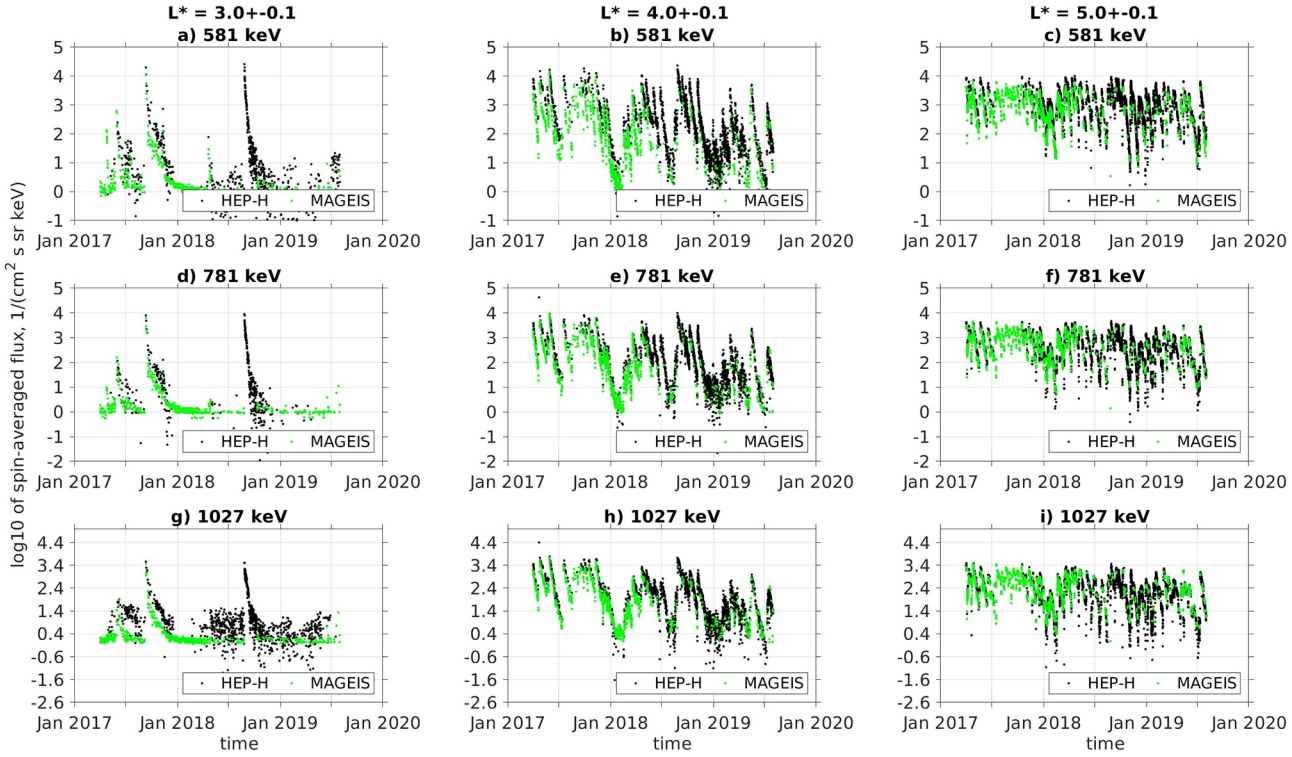

Figure 5. (a–i) Spin-averaged electron flux for a given energy and L* as a function of time plotted in black for Arase HEP-H and green for RBSPa MagEIS. The panels are ordered by the three energy and L* values plotted.

L* values than it would be if calculated for the flux values themselves. For the interested reader, supporting information Figure S7 provides the Pearson correlation coefficient values for the flux values directly.

The correlation between Arase and RBSP instruments is in general >0.8 once instruments on both satellites reliably measure above the noise floor (L* > 3.6). There is a clear decreasing trend with higher L* as the difference between the maximum equatorial pitch angles sampled by Arase and RBSP increases up to the 10° restriction we impose, and Arase samples slightly higher latitudes.

4. Preliminary Intercalibration

The correlation coefficients in Figure 6 are in general above 0.8, indicating that both Arase and RBSP flux measurements show similar time evolution. Likewise, the L* slices in Figure 5 suggest that measurements evolve similarly for both Arase and RBSP, but slight offsets can be observed. We examine the mean ratio of the RBSP and Arase flux measurements for a given energy channel using the full range of flux values, binned by L* with a bin width of ±0.1. The ratios are calculated by dividing RBSP flux by the equivalent Arase flux. We suggest that, as a simple preliminary approach, these ratios could be applied as intercalibration factors to the measurements.

In Figure 7, the base 10 logarithm of these mean ratios are shown on a grid of L* and base 10 logarithm of energy. Figures 7a–7d shows the ratios for each individual instrument, and Figure 7e presents the ratios across all four Arase instruments, with energy channels arranged into ascending order of energy and the ratio value interleaved. In general the ratios are sufficiently close to 1 (<5 and >0.5) to indicate that there is good agreement in the magnitude of the fluxes. For the HEP-L instrument shown on 7b, the ratio is in general < −2 for measurements at L* < 4. This is caused by the MagEIS data frequently hitting a background threshold that is significantly lower than the background threshold of the HEP-L instrument for those energy and L* ranges, as shown on supporting information Figure S2. On Figure 7e, for some of the energy channels such as 1 MeV, the ratios show a discontinuity from the general trends, presenting as horizontal lines across the figure. This is due to the different instruments having different trends as seen in

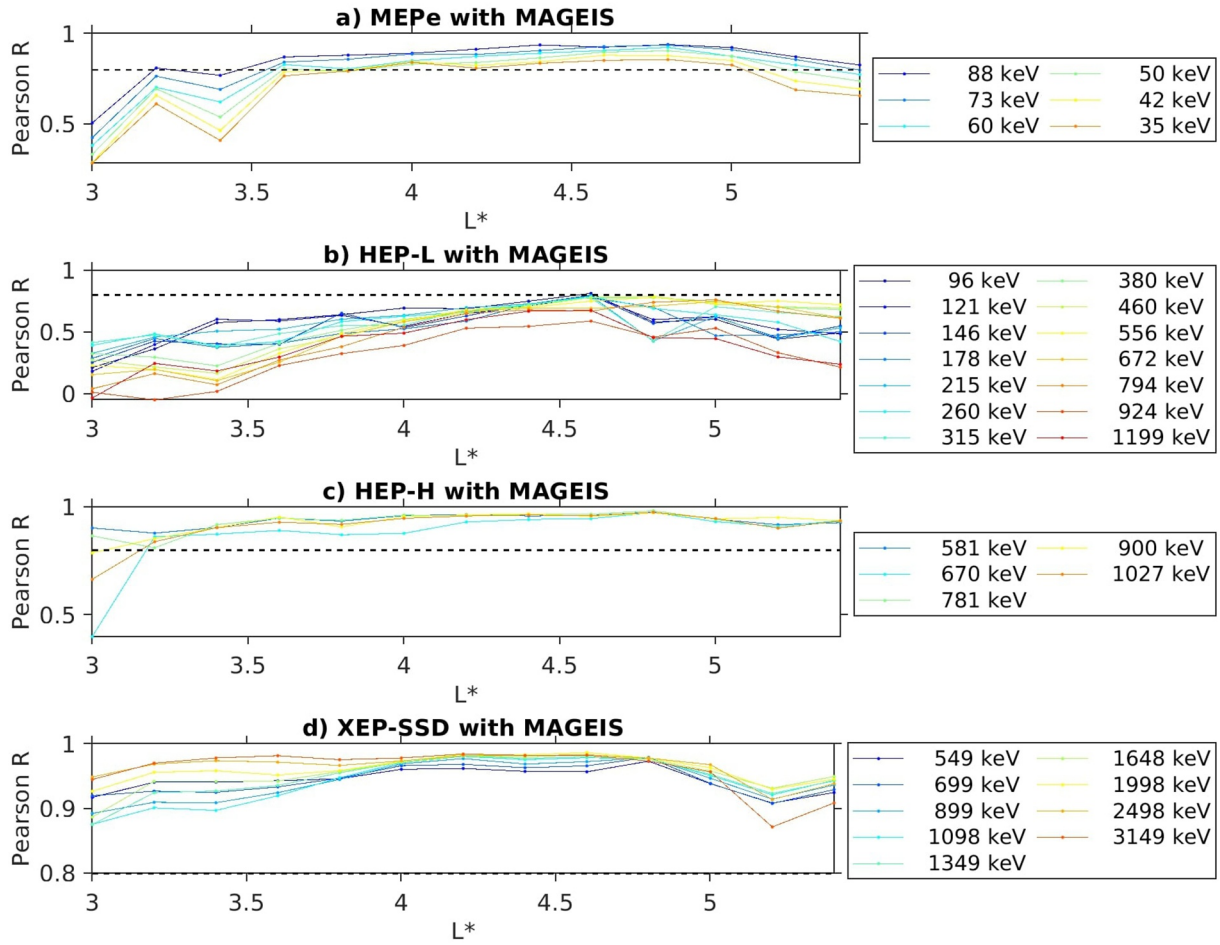

Figure 6. (a–d) Pearson correlation coefficient for the base 10 logarithm of spin-averaged electron flux data plotted as a function of L* in different colors for different energy channels for a given Arase instrument and RBSPa instruments interpolated to the same energy. For reference, a horizontal dashed line marks a correlation of 0.8.

Figures 7a–7d, which will cause discontinuities when we plot all energy channels in ascending order since the instruments have a considerable overlap in their energy range. At higher energies (>1.4 MeV) and L* (>4.4), fluxes measured by RBSP instruments are visibly higher, consistent with Arase being on higher latitudes and observing a different subset of pitch angles, as also demonstrated on Figure 4.

We use flux versus flux scatterplots to show agreement between Arase and RBSP instruments before and after scaling by the mean ratio factors for a given energy channel and L*. We choose to adjust ARASE measurements by multiplying with the intercalibration factors in this study. However, this is solely to have a way of assessing the performance of the intercalibration factors, as we do not have the grounds to establish measurements from either satellite as more reliable than the other. Results for HEP-H are presented for reference as Figure 8, the rest of the Arase electron instruments are shown in supporting information (Figures S4–S6). At higher energies (>1.4 MeV), the not intercalibrated flux from Arase is lower than RBSP at $L^* > 4$. The difference between the measurements is reduced after the intercalibration factors are applied. Arase measures higher flux than RBSP for energies <800 keV. As a result, at these energies Arase measurements remain closer to RBSP measurements even when Arase is at higher latitudes than RBSP. The intercalibration factor has little to no effect on the agreement between MEPe and MagEIS.

As a more quantitative measure for the effectiveness of the intercalibration, the percentage of individual flux measurements from Arase that are within a factor of 5 of corresponding flux measurements from RBSP both before and after the intercalibration factors are applied is shown on Figure 9. The intercalibration factor is particularly effective in the $3.5 < L^* < 4.5$ range for the HEP-H instrument. This metric once again

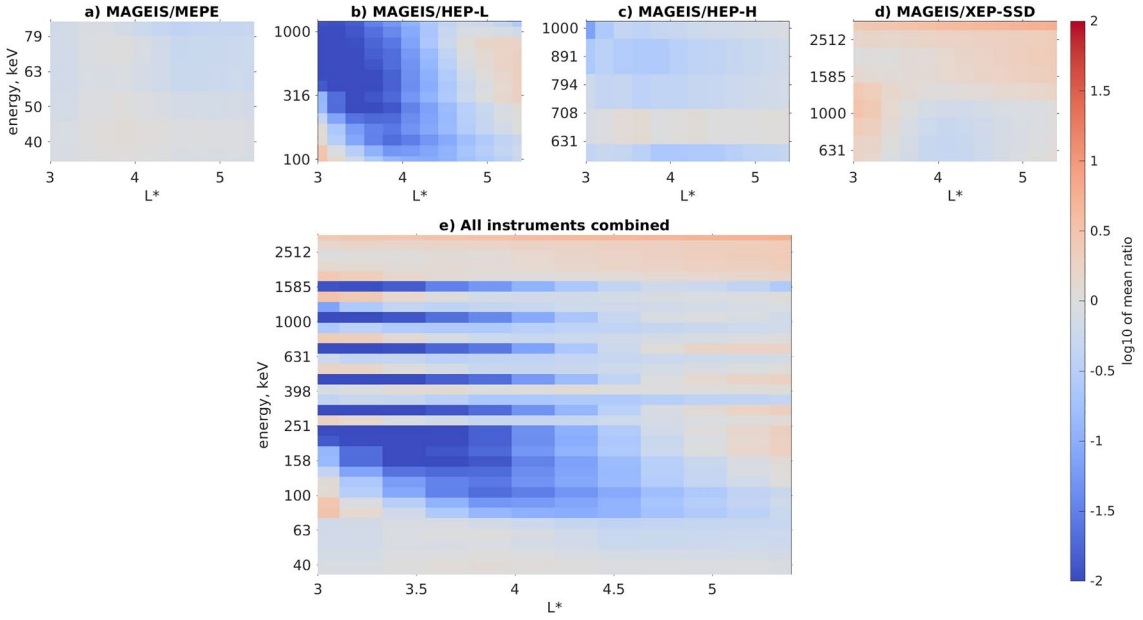

Figure 7. (a–d) Base 10 logarithm of the mean ratio between spin-averaged electron fluxes from an Arase instrument and RBSPa instruments interpolated to the same energy channel definitions, plotted as a function of L* and base 10 logarithm of energy. (e) All ratios shown on the previous four panels, with energy channels from all four instruments arranged into ascending order in energy and the ratio values interleaved. The energy axes on all panels are plotted using a logarithmic scale.

shows that an energy- and L*-dependent intercalibration factor does not capture the cause of differences between MEPe and MagEIS measurements. Use of the intercalibration factor improves the agreement between Arase and RBSP, or at least keeps the percentage of Arase data points within a factor of 5 of RBSP similar for the entire overlap period between the missions.

5. Discussion

Comparisons using spin-averaged data from the Arase and RBSP missions offer insight into the similarities and differences between the two data sets. As discussed in Friedel et al. (2005), spin-averaged comparisons using L* computed for a local 90° pitch angle channel (generally the peak of the pitch angle distribution) also include an error in L* due to drift shell splitting (Roederer, 1967). These errors cannot in principle be quantified without knowledge of the pitch angle distributions at each measurement time, but we can decrease the variation due to Arase sampling higher latitudes by restricting comparisons to measurements where the maximum equatorial pitch angles are similar between the two spacecraft (Friedel et al., 2005, also employed in this study).

Since the calculation of L* also depends on the choice of a magnetic field model, field model inaccuracies make L* computation more challenging and introduce a further source of error when comparing the Arase and RBSP data at L* conjunctions. In this study we chose the T89 model as an example of a less computationally intensive model that nevertheless shows good accuracy up to Kp < 5 (Tsyganenko, 1989), as Kp < 5 held for 98.6% of the studied interval.

At the time of writing, there are no background corrected data products available for the higher energy Arase instruments (HEP, XEP), therefore we use uncorrected MagEIS data for the comparisons, and in doing so implicitly assume that instruments from the two missions are contaminated similarly and have a similar background threshold. Figures 7a–7c demonstrate that at lower energies (<800 keV) and lower L*, Arase fluxes are in general higher than RBSP fluxes. Figures 5a, 5d and 5g also show faster decay times for RBSP fluxes after the enhancements at L* = 3 (most noticeably at Figure 5a, 781 keV), and that the noise threshold across the two missions is different. Since the <800 keV energy range is where Claudepierre et al. (2015) showed background effects to be particularly relevant for MagEIS measurements, this indicates

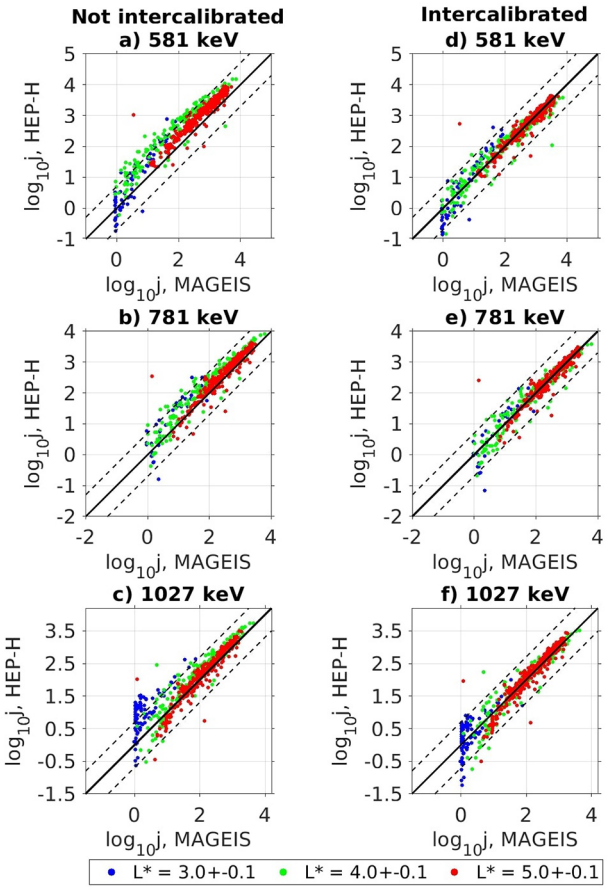

Figure 8. (a–f) Spin-averaged electron flux (latitude restricted as described in Section 2) from Arase HEP-H plotted against spin-averaged electron flux from an RBSPa instrument at three energies, with colors blue, green, and red denoting data at L* = 3, 4, and 5, respectively. For reference, the continuous black line marks one-to-one correspondence, and the dashed black lines show agreement within a factor of 5. Panels (a–c) were produced with data from HEP-H without the intercalibration factors, while panels (d–f) were produced using HEP-H data with the intercalibration factors applied.

that the background corrections required by the two missions may be different. Spin-averaged HEP data are produced by averaging 3-D flux data over all directions, and therefore include data from azimuthal channels which have yet to establish appropriate background correction due to a lack of necessary data samples.

As shown in Figures 4a–4c, 7, S1, and S7, at energies <300 keV the Arase and RBSP fluxes are similar in magnitude but show more scatter in flux. Figures 9a–9c and S4 further demonstrate that the intercalibration factors derived from mean ratios of fluxes at L* conjunctions do not make a noticeable difference in the agreement between Arase and RBSP fluxes at these energies. This is very likely due to the fact that at these energies, electric field effects can significantly influence the electron population and the flux shows a strong dependence on magnetic local time (MLT) during geomagnetically active time periods (Allison et al., 2017). Since our current study does not bin the data in MLT, the derived intercalibration factors are not MLT-dependent. A more detailed investigation establishing intercalibration factors as a function of energy, L*, MLT, and potentially geomagnetic activity, is therefore expected to improve the performance of the intercalibration in this energy range, and is left as a subject for a future study.

6. Conclusions

We compared fluxes from Arase and RBSP at similar energies binned by L* and calculated the Pearson correlation coefficient for the energies and L* studied. As a preliminary intercalibration, we used the mean ratio between Arase and RBSP fluxes at the same L* and energy to improve agreement between Arase and RBSP fluxes, and assessed the performance of this intercalibration. We note that some of the differences between the Arase and RBSP fluxes are not a result of instrument effects, but rather due to the spacecraft sampling populations separated in MLT or pitch angle.

MEPe, HEP-H, HEP-L, XEP-SSD, and MAGEIS in general show a good correlation at energies above 300 keV and L* > 3. The correlation is highest when Arase is close to the magnetic equator, and the instruments from the two missions therefore sample a similar range of equatorial pitch angles. Additionally, fluxes at the same energy from the two missions are typically comparable in magnitude.

Intercalibration via energy- and L*-dependent factors improves the agreement between Arase and RBSP instruments, particularly at energies >1.4 MeV. Taking MLT, magnetic latitude, and/or geomagnetic activity into account is expected to improve the performance of such intercalibration factors even further and is a viable approach for further studies.

The intercalibrated Arase data set can be used in data assimilation studies or radiation belt forecasting to improve prediction quality, provide initial and boundary conditions, or act as a reference for validating model output. Intercalibrated Arase measurements can also serve as a basis for comparisons of simulation results with other missions, and further enable study of phenomena that require multiple satellites to observe, such as particle transport in the radiation belts.

Data Availability Statement

RBSP spin-averaged data files were produced using data release v04 for MagEIS and release v03 for REPT from https://rbsp-ect.newmexicoconsortium.org/data_pub/. Science data of the ERG (Arase) satellite were obtained from the ERG Science Center operated by ISAS/JAXA and ISEE/Nagoya University (https://ergsc.

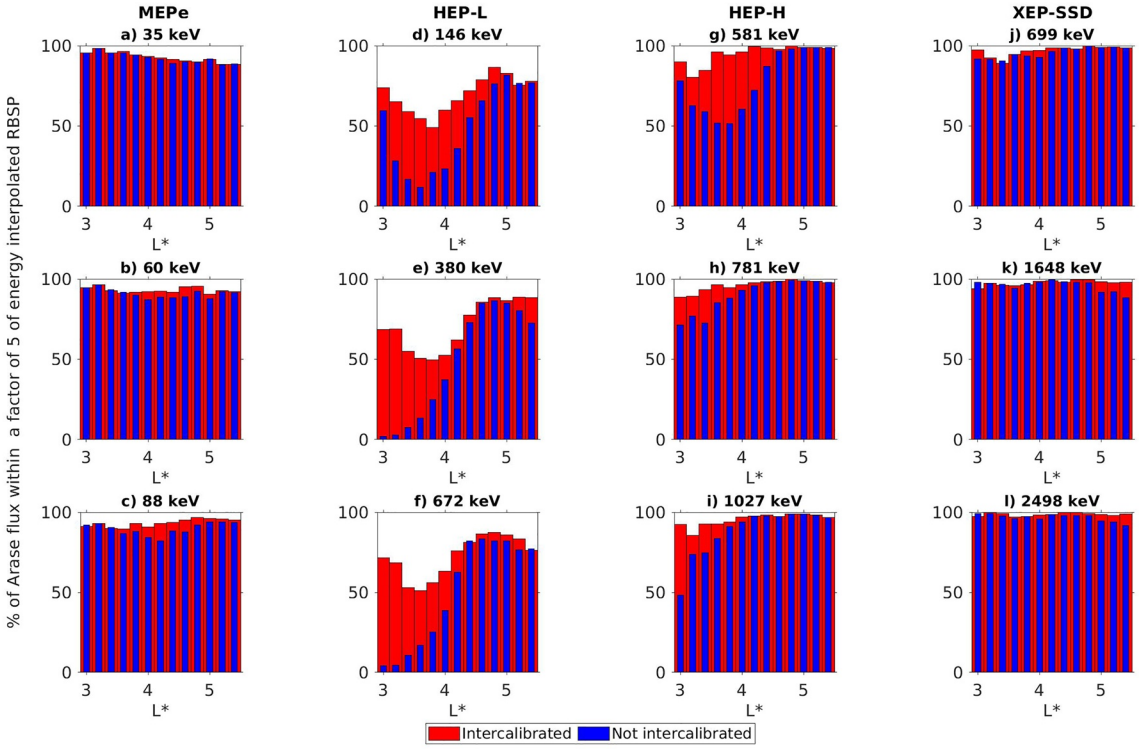

Figure 9. Effect of the intercalibration on the agreement between Arase and RBSPa spin-averaged electron flux values. (a–l) percentage of Arase spin-averaged flux measurements within a factor of 5 of corresponding RBSPa spin-averaged flux measurements at the same energy and L* as a function of L* for three energies on each of the four Arase electron instruments. The percentage calculated using not intercalibrated Arase data is shown in blue, while the percentage calculated using Arase data with the mean ratio factors applied is shown in red.

isee.nagoya-u.ac.jp/index.shtml.en, Miyoshi, Hori, et al. (2018), in particular https://ergsc.isee.nagoya-u.ac.jp/data/ergsc/satellite/erg/). The present study analyzed HEP-L2 v03_01 data (DOI: 10.34515/DATA.ERG-01001), MEP-e-L2 v01_02 data (DOI: 10.34515/DATA.ERG-02001), XEP-l2 v01_00 data (DOI: 10.34515/DATA.ERG-00001), and Orbit L2 v03 data (DOI: 10.34515/DATA.ERG-12000). L* is computed using the IRBEM library (https://sourceforge.net/projects/irbem/) for the T89 magnetic field model, for a local 90° pitch angle channel.

Acknowledgments
We would like to thank Geoff Reeves and Alexander Boyd for their insightful comments on this study. This project was supported by the Recruiting Initiative of the Helmholtz-Gemeinschaft (HGF) 10.13039/5011 00001666. We would like to acknowledge funding received from the European Union's Horizon 2020 research and innovation programme under Grant Agreement 870452 (PAGER), the Deutsche Forschungsgemeinschaft (DFG) with funding through Grant CRC 1294 "Data Assimilation" Project B06, and funding from DFG Project 434829450 (SPEACH).The authors acknowledge use of NASA/GSFC's Space Physics Data Facility's OMNIWeb (or CDAWeb or ftp) service, and OMNI data for Kp.

References

Agapitov, O. V., Mourenas, D., Artemyev, A. V., & Mozer, F. S. (2016). Exclusion principle for very oblique and parallel lower band chorus waves. *Geophysical Research Letters*, *43*(21), 11112–11120. https://doi.org/10.1002/2016gl07125

Allison, H. J., Horne, R. B., Glauert, S. A., & Zanna, G. D. (2017). The magnetic local time distribution of energetic electrons in the radiation belt region. *Journal of Geophysical Research: Space Physics*, *122*(8), 8108–8123. https://doi.org/10.1002/2017ja024084

Baker, D. N., Kanekal, S. G., Hoxie, V. C., Batiste, S., Bolton, M., Li, X., et al. (2012). The relativistic electron-proton telescope (REPT) instrument on board the radiation belt storm probes (RBSP) spacecraft: Characterization of Earth's radiation belt high-energy particle populations. *Space Science Reviews*, *179*(1–4), 337–381. https://doi.org/10.1007/s11214-012-9950-9

Baker, D. N., Kanekal, S. G., Hoxie, V. C., Henderson, M. G., Li, X., Spence, H. E., et al. (2013). A long-lived relativistic electron storage ring embedded in Earth's outer Van Allen belt. *Science*, *340*(6129), 186–190. https://doi.org/10.1126/science.1233518

Baker, D. N., Zhao, H., Li, X., Kanekal, S. G., Jaynes, A. N., Kress, B. T., et al. (2019). Comparison of Van Allen Probes energetic electron data with corresponding GOES-15 measurements: 2012–2018. *Journal of Geophysical Research: Space Physics*, *124*(12), 9924–9942. https://doi.org/10.1029/2019ja027331

Blake, J. B., Carranza, P. A., Claudepierre, S. G., Clemmons, J. H., Crain, W. R., Dotan, Y., et al. (2013). The Magnetic Electron Ion Spectrometer (MagEIS) instruments aboard the Radiation Belt Storm Probes (RBSP) spacecraft. *Space Science Reviews*, *179*(1–4), 383–421. https://doi.org/10.1007/s11214-013-9991-8

Boyd, A. J., Reeves, G. D., Spence, H. E., Funsten, H. O., Larsen, B. A., Skoug, R. M., et al. (2019). RBSP-ECT combined spin-averaged electron flux data product. *Journal of Geophysical Research: Space Physics*, *124*(11), 9124–9136. https://doi.org/10.1029/2019ja026733

Boyd, A. J., Turner, D. L., Reeves, G. D., Spence, H. E., Baker, D. N., & Blake, J. B. (2018). What causes radiation belt enhancements: A survey of the Van Allen Probes era. *Geophysical Research Letters*, *45*(11), 5253–5259. https://doi.org/10.1029/2018gl077699

Breneman, A. W., Halford, A., Millan, R., McCarthy, M., Fennell, J., Sample, J., et al. (2015). Global-scale coherence modulation of radiation-belt electron loss from plasmaspheric hiss. *Nature*, *523*(7559), 193–195. https://doi.org/10.1038/nature14515

Cervantes, S., Shprits, Y. Y., Aseev, N. A., & Allison, H. J. (2020). Quantifying the effects of EMIC wave scattering and magnetopause shadowing in the outer electron radiation belt by means of data assimilation. *Journal of Geophysical Research: Space Physics*, *125*(8), e2020JA028208. https://doi.org/10.1029/2020ja028208

Chen, Y. (2005). Multisatellite determination of the relativistic electron phase space density at geosynchronous orbit: Methodology and results during geomagnetically quiet times. *Journal of Geophysical Research*, *110*(A10), A10210. https://doi.org/10.1029/2004ja010895

Claudepierre, S. G., O'Brien, T. P., Blake, J. B., Fennell, J. F., Roeder, J. L., Clemmons, J. H., et al. (2015). A background correction algorithm for Van Allen Probes MagEIS electron flux measurements. *Journal of Geophysical Research: Space Physics*, *120*(7), 5703–5727. https://doi.org/10.1002/2015ja021171

Davis, G. (2007). History of the NOAA satellite program. *Journal of Applied Remote Sensing*, *1*(1), 012504. https://doi.org/10.1117/1.2642347

Fennell, J. F., Claudepierre, S. G., Blake, J. B., O'Brien, T. P., Clemmons, J. H., Baker, D. N., et al. (2015). Van Allen Probes show that the inner radiation zone contains no MeV electrons: ECT/MagEIS data. *Geophysical Research Letters*, *42*(5), 1283–1289. https://doi.org/10.1002/2014gl062874

Foster, J. C., Erickson, P. J., Omura, Y., Baker, D. N., Kletzing, C. A., & Claudepierre, S. G. (2017). Van Allen Probes observations of prompt MeV radiation belt electron acceleration in nonlinear interactions with VLF chorus. *Journal of Geophysical Research: Space Physics*, *122*(1), 324–339. https://doi.org/10.1002/2016ja023429

Friedel, R. H. W., Bourdarie, S., & Cayton, T. E. (2005). Intercalibration of magnetospheric energetic electron data. *Space Weather*, *3*(9), S09B04. https://doi.org/10.1029/2005sw000153

Funsten, H. O., Skoug, R. M., Guthrie, A. A., MacDonald, E. A., Baldonado, J. R., Harper, R. W., et al. (2013). Helium, Oxygen, Proton, and Electron (HOPE) mass spectrometer for the Radiation Belt Storm Probes mission. *Space Science Reviews*, *179*(1–4), 423–484. https://doi.org/10.1007/s11214-013-9968-7

Higashio, N., Takashima, T., Shinohara, I., & Matsumoto, H. (2018). The extremely high-energy electron experiment (XEP) onboard the Arase (ERG) satellite. *Earth, Planets and Space*, *70*(1). https://doi.org/10.1186/s40623-018-0901-x

Kasahara, S., Yokota, S., Mitani, T., Asamura, K., Hirahara, M., Shibano, Y., & Takashima, T. (2018). Medium-energy particle experiments—Electron analyzer (MEP-e) for the exploration of Energization and Radiation in Geospace (ERG) mission. *Earth, Planets and Space*, *70*(1). https://doi.org/10.1186/s40623-018-0847-z

Kazama, Y., Wang, B.-J., Wang, S.-Y., Ho, P. T. P., Tam, S. W. Y., Chang, T.-F., et al. (2017). Low-energy particle experiments–electron analyzer (LEPe) onboard the Arase spacecraft. *Earth, Planets and Space*, *69*(1), 165. https://doi.org/10.1186/s40623-017-0748-6

Kellerman, A. C., Shprits, Y. Y., Kondrashov, D., Subbotin, D., Makarevich, R. A., Donovan, E., & Nagai, T. (2014). Three-dimensional data assimilation and reanalysis of radiation belt electrons: Observations of a four-zone structure using five spacecraft and the VERB code. *Journal of Geophysical Research: Space Physics*, *119*(11), 8764–8783. https://doi.org/10.1002/2014ja020171

Li, W., & Hudson, M. (2019). Earth's Van Allen radiation belts: From discovery to the Van Allen Probes era. *Journal of Geophysical Research: Space Physics*, *124*(11), 8319–8351. https://doi.org/10.1029/2018ja025940

Miyoshi, Y., Hori, T., Shoji, M., Teramoto, M., Chang, T. F., Segawa, T., et al. (2018). The ERG Science Center. *Earth, Planets and Space*, *70*(1), 96. https://doi.org/10.1186/s40623-018-0867-8

Miyoshi, Y., Shinohara, I., Takashima, T., Asamura, K., Higashio, N., Mitani, T., et al. (2018). Geospace exploration project ERG. *Earth, Planets and Space*, *70*(1), 101. https://doi.org/10.1186/s40623-018-0862-0

Ni, B., Shprits, Y., Hartinger, M., Angelopoulos, V., Gu, X., & Larson, D. (2011). Analysis of radiation belt energetic electron phase space density using THEMIS SST measurements: Cross-satellite calibration and a case study. *Journal of Geophysical Research*, *116*(A3), A03208. https://doi.org/10.1029/2010ja016104

Reeves, G. D., Belian, R. D., Cayton, T. C., Henderson, M. G., Christensen, R. A., McLachlan, P. S., & Ingraham, J. C. (1997). Using Los Alamos geosynchronous energetic particle data in support of other satellite missions. In M., Lockwood, M. N., Wild, & H. J., Opgenoorth (Eds.), *Satellite-ground based coordination sourcebook* (Vol. 1198, p. 281). ESA Publications.

Roederer, J. G. (1967). On the adiabatic motion of energetic particles in a model magnetosphere. *Journal of Geophysical Research*, *72*(3), 981–992. https://doi.org/10.1029/jz072i003p00981

Roussos, E., Dialynas, K., Krupp, N., Kollmann, P., Paranicas, C., Roelof, E. C., et al. (2020). Long- and short-term variability of galactic cosmic-ray radial intensity gradients between 1 and 9.5 au: Observations by Cassini, BESS, BESS-polar, PAMELA, and AMS-02. *The Astrophysical Journal*, *904*(2), 165. https://doi.org/10.3847/1538-4357/abc346

Shprits, Y. Y., & Michaelis, I. (2018). *Data-assimilative radiation belt forecast*. https://spaceweather.gfz-potsdam.de/products-data/forecasts/data-assimilative-radiation-belt-forecast

Smirnov, A. G., Kronberg, E. A., Daly, P. W., Aseev, N. A., Shprits, Y. Y., & Kellerman, A. C. (2020). Adiabatic invariants calculations for Cluster mission: A long-term product for radiation belts studies. *Journal of Geophysical Research: Space Physics*, *125*(2), e2019JA027576. https://doi.org/10.1029/2019ja027576

Smirnov, A. G., Kronberg, E. A., Latallerie, F., Daly, P. W., Aseev, N., Shprits, Y. Y., et al. (2019). Electron intensity measurements by the Cluster/RAPID/IES instrument in Earth's radiation belts and ring current. *Space Weather*, *17*(4), 553–566. https://doi.org/10.1029/2018sw001989

Stratton, J. M., Harvey, R. J., & Heyler, G. A. (2013). Mission overview for the Radiation Belt Storm Probes mission. *Space Science Reviews*, *179*(1–4), 29–57. https://doi.org/10.1007/s11214-012-9933-x

Tsyganenko, N. (1989). A magnetospheric magnetic field model with a warped tail current sheet. *Planetary and Space Science*, *37*(1), 5–20. https://doi.org/10.1016/0032-0633(89)90066-4

Vampola, A. L. (1992). Combined release and radiation effects satellite. *Journal of Spacecraft and Rockets*, *29*(4), 555. https://doi.org/10.2514/3.55640

Xiao, F., Yang, C., He, Z., Su, Z., Zhou, Q., He, Y., et al. (2014). Chorus acceleration of radiation belt relativistic electrons during March 2013 geomagnetic storm. *Journal of Geophysical Research: Space Physics*, *119*(5), 3325–3332. https://doi.org/10.1002/2014ja019822

Xiao, F., Yang, C., Su, Z., Zhou, Q., He, Z., He, Y., et al. (2015). Wave-driven butterfly distribution of Van Allen belt relativistic electrons. *Nature Communications*, *6*(1), 8590. https://doi.org/10.1038/ncomms9590

Yuan, C.-J., & Zong, Q.-G. (2019). The efficiency of coronal mass ejection with different IMF preconditions on the production of mega electron volt electron content in the outer radiation belt. *Journal of Geophysical Research: Space Physics*, *124*(5), 3222–3235. https://doi.org/10.1029/2018ja026263